Pergamon

Int. J. Heat Mass Transfer. Vol. 39, No. 17, pp. 3695–3706, 1996

0017–9310/96 $15.00 + 0.00

PII: S0017–9310(96)00027–0

Heat transfer and flow structures in an excited circular impinging jet

TIANSHU LIU and J. P. SULLIVAN

School of Aeronautics and Astronautics, Purdue University, West Lafayette, IN 47906, U.S.A.

(*Received* 12 *October* 1995 *and in final form* 9 *December* 1995)

Abstract—Flow structures and heat transfer are investigated experimentally in an excited circular impinging jet with small nozzle-to-plate spacing ($H/D \leqslant 2$). The local heat transfer in the wall–jet region is found to be sensitive to the excitation frequency. Enhancement and reduction of the local heat transfer in the wall–jet region can be attained by forcing the impinging jet near the natural frequency and its subharmonic, respectively. The relationship between the vortical structures and local heat transfer is studied by the means of flow visualization, heat transfer spectra and correlation between velocity and heat transfer. Copyright © 1996 Elsevier Science Ltd.

INTRODUCTION

Impinging jets are widely used in industry as a high-performance technique for heating, cooling and drying materials. Numerous studies of jet impingement heat transfer have been published, and comprehensive reviews have been presented by Viskanta [1] and Jambunathan *et al.* [2]. It has long been recognized that small-scale free-stream turbulence enhances the stagnation-point heat transfer [3–6]. The large-scale organized structures in an impinging jet have been studied by several authors from a standpoint of fluid mechanics [7–10]. Nonetheless, effects of the large-scale organized vortical structures on the impingement heat transfer are not fully understood. Özdemir and Whitelaw [11] report that large stationary vortical structures cause local augmentation of the convective heat transfer coefficient. However, other experiments indicate that the large-scale organized vortical structures do not effectively increase the local heat transfer [12] and sometimes can lead to a reduction in the local heat transfer [13]. Therefore, an attempt is needed to clarify the effects of the large-scale organized vortical structures on the impingement heat transfer.

This paper focuses on the relationship between the flow structures and local heat transfer in an excited circular impinging jet. The dependencies of the local heat transfer distributions on the excitation frequency are examined at different nozzle-to-plate spacings. It is found that the local heat transfer in the wall–jet region can be significantly enhanced by the excitation close to the natural frequency and reduced by the excitation close to the subharmonic of the natural frequency. The physical mechanisms behind the heat transfer enhancement and reduction phenomena are studied by means of flow visualization, heat transfer spectra and correlation between velocity and heat transfer. The local heat transfer reduction results from the unsteady separation induced by strong well-organized vortices formed in the stable vortex pairing. In contrast, the local heat transfer enhancement is caused by chaotic 'lump eddy' with a great deal of the random turbulence.

EXPERIMENTAL APPARATUS AND TECHNIQUES

A schematic diagram of the variable-speed air jet facility and the coordinate system is shown in Fig. 1. The facility consists of two settling chambers. The air flow from a motor-driven centrifugal blower enters the first rectangular settling chamber ($254 \times 533 \times 483$ mm) and then passes through the second chamber which is a 178 mm long cylinder tube of 48 mm diameter. A 25 mm long contoured nozzle is mounted at the end of the tube. The nozzle exit diameter D is 12.7 mm and the contraction ratio is 5.2. A loudspeaker attached to one side of the first chamber induces organ-pipe resonance in the chamber, producing plane-wave excitation at the jet exit. Since the loudspeaker is located directly opposite the nozzle on the other side of the chamber, the excitation perturbation is axisymmetric. The initial excitation level in the shear layer was measured using a hot-wire at 0.5 mm from the nozzle lip in a fixed speaker power 8 W. The perturbation velocity u'/U_0 varies between 0.05 and 0.18% in a frequency range from 600 to 2500 Hz. The average excitation level is about 0.1%.

To measure the local convective heat transfer coefficient h, the air jet impinges on a 0.0254 mm thick, 115 mm wide, 130 mm long stainless steel sheet that is heated by passing 25 A electric current. The sheet is stretched tautly by springs over two 12.5 mm diameter aluminum rods, which serve as electrodes. The heat flux Q_s from the heated sheet surface is 2756 W m^{-2}. Then, $h = Q_s/(T_s - T_\infty)$, where T_s is the surface temperature of the heated sheet and T_∞ is the ambient temperature. Since the maximum value of T_s is less than 100°C, the radiation heat loss is neglected. The

NOMENCLATURE

c_p	specific heat [J kg^{-1} K^{-1}]
D	nozzle diameter [m]
E	output voltage of anemometer [Volt]
E_0	E without flow [Volt]
E'	voltage fluctuation [Volt]
f_n	natural frequency [Hz]
f_e	excitation frequency [Hz]
h	local convective heat transfer coefficient [W m^{-2} K^{-1}]
H	nozzle-to-plate spacing [m]
I	fluorescence intensity [J s^{-1}]
k	thermal conductivity of air [W m^{-1} K^{-1}]
Nu	Nusselt number, hD/k
Nu_0	stagnation-point Nusselt number
Pr	Prandtl number, $\rho c_p \nu/k$
Q	local convective heat transfer rate [W m^{-2}]
Q_0	convective heat transfer rate at stagnation-point [W m^{-2}]
Q_s	heat flux from heated steel sheet surface [W m^{-2}]
Q'	local convective heat transfer fluctuation [W m^{-2}]
r	radial coordinate [m]
$R_{Q'u'}$	correlation coefficient, $\overline{Q'(t+\tau,0)u'(t,y)}/(Q'u')$
Re_D	Reynolds number, $U_0 D/\nu$
T	temperature [°C]
T_r	reference temperature [°C]
T_s	temperature of heated steel sheet surface [°C]
T_∞	ambient temperature [°C]
T'	temperature fluctuation [°C]
U_0	jet exit velocity [m s^{-1}]
u	streamwise velocity [m s^{-1}]
u'	streamwise fluctuating velocity [m s^{-1}]
v'	fluctuating velocity normal to wall [m s^{-1}]
x	streamwise cordinate in free jet [m]
y	coordinate normal to wall [m].

Greek symbols

$-\alpha_i$	spatial amplification rate [m^{-1}]
η	factor of heat transfer enhancement, $Q(f_e)/Q(f_e=0)-1$
ν	kinematic viscosity [m^2 s^{-1}]
θ	momentum thickness [m]
θ_0	initial momentum thickness [m]
ρ	density of air [kg m^{-3}].

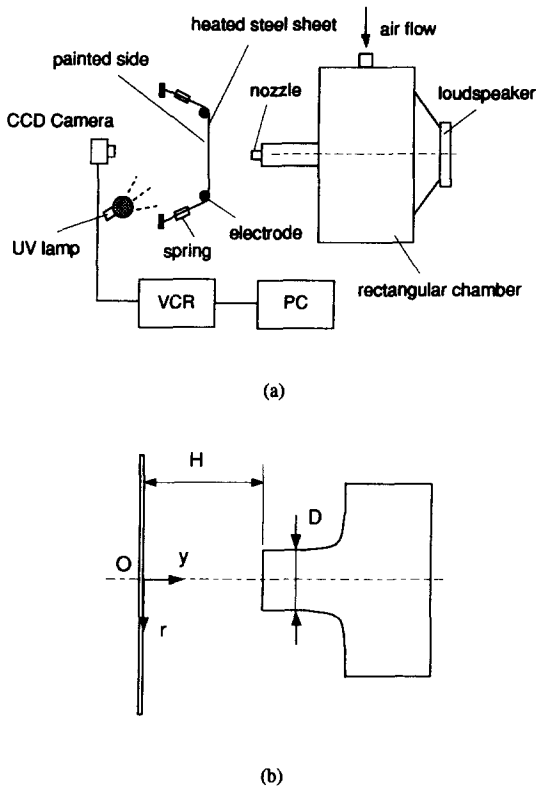

Fig. 1. Experimental set-up: (a) jet facility, (b) coordinate system.

maximum deformation of the sheet due to low speed jet impingement is less than 0.1 mm. Note that the jet impingement cooling could cause spatial variation of the sheet resistivity and consequently lead to non-uniform heating. The measurements of the spatial variations of the sheet resistance show that the non-uniformity of heating is less than 4%. Since the heated stainless steel sheet is vertical, it is necessary to estimate the effect of the buoyancy force. In a typical test condition, $Gr_L/Re_L^2 = 7.8 \times 10^{-4}$, where the Grashof number, $Gr_L = g\beta(T_s - T_\infty)L^3/\nu^2$, and the Reynolds number, $Re_L = U_0 L/\nu$. In above estimate, the characteristic length L is the sheet width, the typical temperature difference $T_s - T_\infty$ is 40°C, the jet exit velocity U_0 is 14 m s^{-1}, and other parameters have the standard values for the quiescent air. Obviously, since $Gr_L/Re_L^2 \ll 1$, the buoyancy effect is small and can be neglected [14].

The temperature-sensitive fluorescent paint technique was used to measure surface temperature T_s. Fluorescence is a photoluminescence process whereby the molecules of a fluorophore substance absorb light of a particular wavelength and emit radiation of a longer wavelength by losing their excitation energy. The fluorescence intensity can be affected by so-called thermal quenching and consequently depends on temperature. Hence, temperature can be measured by detecting the fluorescence intensity $I(T)$. The principles of the fluorescent paint technique are discussed in detail by Liu *et al.* [15–17].

In this study, a fluorescent paint, europium thenoyltrifluoroacetonate (EuTTA) in a polymer solution (dope for painting model airplane) was used. For the EuTTA-dope paint, the calibration relation between temperature and relative fluorescent intensity $I(T)/I(T_r)$ was experimentally determined, where the reference temperature T_r equals the ambient temperature (22°C). A fourth-order polynomial fit of calibration data is given by

$$I(T)/I(T_r) = \sum_{n=0}^{4} a_n T^n$$

where $a_0 = 1.8723459$, $a_1 = -0.0303419$, $a_2 = -8.657407 \times 10^{-4}$, $a_3 = 2.308471 \times 10^{-5}$ and $a_4 = -1.40501 \times 10^{-7}$. The EuTTA-dope paint (about 10 μm thick) was coated on the 0.05 mm thick white Mylar film attached on the backside (relative to the impingement side) of the stainless steel sheet. The illumination source for exciting the fluorophore molecules was provided by an ultraviolet lamp. The fluorescence intensity image was taken by a CCD video camera and recorded by a VCR. Then, the image was digitized by a frame grabber with 512×512 pixel spatial resolution and was converted into the surface temperature map using the calibration relation. Once T_s is known, the local heat transfer coefficient h can be calculated from the definition $h = Q_s/(T_s - T_\infty)$. The accuracy of the fluorescent paint technique has been estimated by Liu *et al.* [18]. Error in temperature measurement using the EuTTA-dope paint is ± 0.8°C. The low value of $T_s - T_\infty$ is about 10°C. The uncertainty of Q_s is about $\pm 4\%$. Hence, according to the root-sum-square method, the uncertainty in calculating h is about $\pm 9\%$.

The flush-mount hot-film sensor (TSI 1237) was adapted for measurement of the surface heat transfer fluctuation. The sensor is mounted on a movable plastic target plate that is traversed relative to the nozzle in the transverse direction. From the thermal equilibrium relation of the hot-film element connected with a constant temperature anemometer, the convective heat transfer rate Q from the hot-film can be expressed as $Q = C(E^2 - E_0^2)$, where E is the output voltage of the anemometer, E_0 is the voltage when $Q = 0$ and C is a constant. In shear flow, the convective heat transfer rate Q from the film is proportional to the cubic root of the wall shearing stress [19, 20]. Hence, measurements of Q also reveal the local properties of flow near the surface. For small heat transfer fluctuations, $Q' \approx 2CEE'$, where Q' is the root-mean-square (r.m.s.) fluctuation of the convective heat transfer rate and E' is the r.m.s. fluctuation of the voltage.

FLOW CHARACTERISTICS

Free jet

Velocity measurements for a free jet were carried out using a single hot-wire probe in order to provide information about the free jet itself. The centerline velocity decreases slightly with the streamwise distance x and the potential core remains when $x/D < 4$. The centerline turbulence intensity is about 0.4% at the exit and reaches a maximum level of 9.5% at $x/D = 5.5$. The boundary layer at the nozzle lip is laminar. The normalized velocity u/U_0 at the nozzle lip measured at different Reynolds numbers ($Re_D = 7170$, 9700 and 12 300) has a near-Blasius profile when a nondimensional coordinate y_1/θ_0 is used, where y_1 is the normal distance from the inner surface of the nozzle, U_0 is the exit velocity and θ_0 is the initial momentum thickness. At $Re_D = 7170$, 9700 and 12 300, the values of θ_0 are 0.172, 0.161 and 0.137 mm, respectively. Since $\theta_0/D \ll 1$, the boundary layer at the nozzle lip is nearly two-dimensional.

The development of the shear layer downstream of the nozzle edge is initially dominated by the Kelvin–Helmholtz instability mechanism. Since $\theta_0 \ll D$, the initial shear layer of a circular jet can be approximated as being a two-dimensional mixing layer. Hence, if the disturbances are small, classical hydrodynamic stability theory can describe satisfactorily the initial evolution of the instability wave in the mixing layer [21]. The instability waves grow exponentially with downstream distance and an important stability characteristic is the spatial amplification rate $-\alpha_i = \mathrm{d}[\ln(u'/U_0)]/\mathrm{d}x$, where α_i is the imaginary part of the complex wave number, x is the streamwise coordinate and u' is the streamwise perturbation velocity. The spatial amplification rate is a function of the frequency. By introducing a weak perturbation, $-\alpha_i$ was determined experimentally within the linear unstable region ($x/D = 0.25$–0.63) at $Re_D = 12\,300$. As shown in Fig. 2(a), the dimensionless amplification growth rate $-\alpha_i\theta$ depends on the nondimensional excitation frequency $f_e\theta/U_0$, where f_e is the excitation frequency and the local momentum thickness θ is 0.165 mm. The experimental data are in agreement with a theoretical calculation by Monkewitz and Huerre [22] for the Blasius mixing layer. The measured natural frequency f_n of the unexcited jet is 1400 Hz ($f_n\theta/U_0 = 0.016$ or $f_nD/U_0 = 1.23$) at $Re_D = 12\,300$, which coincides with the theoretical value of the most amplified wave. As the shear layer develops and θ grows, the properties of the jet should be scaled by the length scale D. Over a range of $x/D = 0.5$–3.8, the dimensionless natural frequency f_nD/U_0 of the unexcited jet decreases from 1.23 near the exit to 0.61 at $x/D = 2.5$, as shown in Fig. 2(b). The stepwise evolution of the vortex passage frequency is similar to Kibens' results [23] for an excited jet. Although the 'jet column mode' in the test is twice the value of $fD/U_0 = 0.3$ reported by Crow and Champagne [24], it is close to $fD/U_0 = 0.5$ given by Browand and Laufer [25]. In fact, the 'jet column mode' measured in various experiments appears to vary widely from 0.25 to 0.85 [26].

Impinging jet

In contrast with the free jet in which θ_0 and D are the two characteristic length scales, the impinging jet

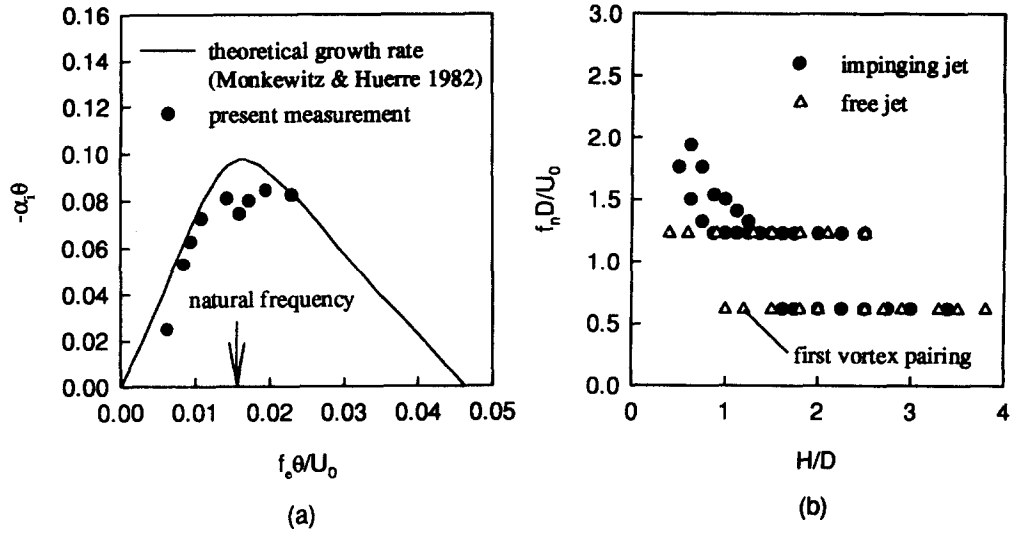

Fig. 2. Frequency characteristics of flow when $Re_D = 12\,300$: (a) initial free jet shear layer spatial amplification rate, (b) natural frequencies of free and impinging jets.

introduces an additional length scale: the nozzle-to-plate spacing H. At small H/D, the natural frequencies of the impinging jet may differ from the free jet because of the presence of the plate. The natural frequency f_n of the unexcited impinging jet was detected by a hot-film sensor flush-mounted on the target plate at $r/D = 0.7$. In Fig. 2(b), the nondimensional natural frequency f_nD/U_0 in the impinging jet is compared with that in the free jet at $Re_D = 12\,300$. The natural frequency of the impinging jet coincides with that of the free jet when $H/D > 1.2$, and tends to increase when H/D becomes smaller. When $H/D = 0.8$–1.2, two peaks can be observed in the power spectrum of the hot-film signal. Their frequencies are different until two modes merge into the dominant mode of the free jet at $H/D = 1.2$. The mechanisms generating the two modes at small H/D are unclear.

The mean local streamwise velocity and r.m.s. fluctuating velocity in the wall-jet region were measured at $r/D = 0.79$, 1.1 and 1.4 when $H/D = 1.125$ and $Re_D = 12\,300$. The mean local streamwise velocity distributions along the normal direction to the wall indicate that the wall–jet thickness is of the order of $D/4$. Here, $D/4$ is the wall–jet thickness at $r/D = 0.5$ for an inviscid axisymmetric impinging jet. The maximum local streamwise velocity u_{max} almost equals the jet exit velocity U_0 in $r/D = 0.79$–1.1. This suggests that the potential core persists in this region, although it is deflected and spread along the radial direction by the target plate. The potential core separates the outer shear layer and the wall boundary layer, constituting a 'sandwich' structure of three flow regimes. The outer shear layer occupies most of the wall–jet. The outer shear layer has an approximate hyperbolic tangent profile $u/u_{max} = 0.5[1 + \tanh(\zeta)]$ at $r/D = 0.79$ and 1.1. Here, the normalized coordinate $\zeta = 2(y_{0.5} - y)/\delta_\omega$, where y is the coordinate normal to the plate wall, $y_{0.5}$ is the location at which $u/u_{max} = 0.5$, and $\delta_\omega = u_{max}/(\partial u/\partial y)_{max}$ is the vorticity thickness. Thus, the outer shear layer exhibits similar features to a two-dimensional mixing layer [21, 26]. When $r/D > 1.1$, due to viscous diffusion, the wall boundary layer merges with the outer shear layer. Therefore, the u profile becomes fully developed and the maximum of u decreases with radial distance. The maximum values of the fluctuating velocity u'/U_0 at $r/D = 0.79$, 1.1 and 1.4 are 0.14, 0.2 and 0.25, respectively.

UNEXCITED AND EXCITED JET IMPINGEMENT HEAT TRANSFER

In the unexcited impinging jet, the stagnation-point heat transfer Nu_0 was measured as a characteristic quantity for comparison with the well-known theoretical solution. When $H/D \leqslant 2$, the flow near the stagnation-point can be described by the laminar boundary-layer solution. For a laminar stagnation-point flow, the theoretical relation between Nu_0 and Re_D is $Nu_0 = CPr^{0.4}\ (D\beta_1/U_0)^{1/2}Re_D^{1/2}$ [27], where $\beta_1 = (dU/dr)_{r=0}$, $Re_D = U_0D/\nu$, U is the velocity of the potential flow outside of the stagnation-point, U_0 is the jet exit velocity and D is the diameter of the nozzle. The constant C is 0.763 for the axisymmetric flow. Based on the potential flow analysis, Shadlesky [28] suggested that the velocity gradient parameter $D\beta_1/U_0 = 3\pi/16$ for an axisymmetric jet. Hence, $Nu_0/(Pr^{0.4}Re_D^{1/2}) = 0.585$. Figure 3 shows the stagnation-point heat transfer as a function of H/D. The experimental data are in good agreement with the theoretical value when $H/D < 2$. As the shear layer develops downstream, the potential core diminishes and the heat transfer data deviate from the theoretical value. The maximum stagnation-point heat transfer is attained for $H/D = 6$–8.

Effects of monochromatic excitation on the surface heat transfer are studied when the average initial exci-

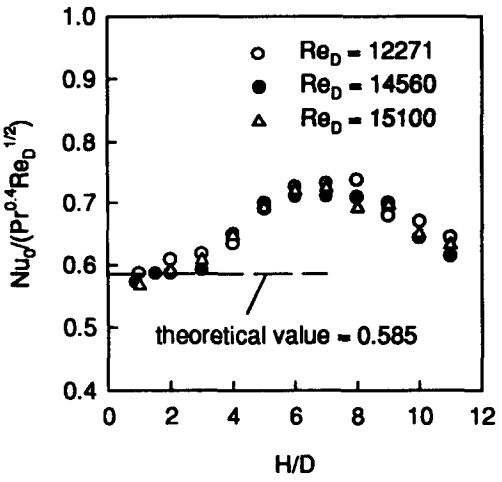

Fig. 3. Stagnation-point heat transfer as a function of H/D.

tation level is fixed at $u'/U_0 = 0.1\%$. Figure 4 shows the two-dimensional Nusselt number (Nu) distributions of the impinging jets for the cases of $f_e = 950$ Hz, 1750 Hz and no excitation when $H/D = 1.125$ and $Re_D = 12\,300$. The two-dimensional heat transfer distributions are obtained using the temperature-sensitive fluorescent paint technique. Clearly, the two-dimensional heat transfer distribution is sensitive to the excitation frequency. The transverse heat transfer distributions in the excited impinging jet are plotted in Fig. 5 against that in the unexcited impinging jet at $H/D = 1.125$. At $f_e = 1750$ Hz, the local heat transfer in the wall–jet region ($1 < r/D < 2$) is considerably enhanced compared with that in the unexcited impinging jet. In contrast, at a lower excitation frequency $f_e = 950$ Hz, the local heat transfer is reduced in the wall–jet region. Near the stagnation-point ($-1 < r/D < 1$), the monochromatic excitation does not significantly affect the time-averaged heat transfer.

In order to characterize the heat transfer enhancement or reduction in a wide domain of the excitation frequencies, a local enhancement factor η is introduced, $\eta = Q(f_e)/Q(f_e = 0) - 1$, where $Q(f_e)$ and $Q(f_e = 0)$ are the local transfer rates of the impinging jet with the excitation and without the excitation, respectively. The positive η indicates the local heat transfer enhancement and the negative η the reduction. The magnitude of η represents the proportion of the enhancement or reduction. Figure 6 shows the frequency-dependence of η obtained with a flush-mount hot-film sensor at a particular radial location $r/D = 1.53$, where the local heat transfer is very sensitive to the excitation. Significant heat transfer enhancement can be observed in a certain range of frequencies when $0.875 \leqslant H/D \leqslant 2$. The maximum enhancement of the local heat transfer is about 10%. When $H/D \leqslant 0.625$, no obvious heat transfer enhancement is detected at any excitation frequency. The frequency band in which the heat transfer reduction is attained becomes narrow and eventually diminishes as H/D increases. When $H/D > 3$, neither enhancement nor reduction of the local heat transfer is found. In Fig. 6, the natural frequency f_n of the impinging jet is marked by an arrow. An important observation is that the heat transfer enhancement may occur when f_e is close to f_n and the heat transfer reduction may happen when f_e is close to $f_n/2$. The causes of the heat transfer enhancement and reduction will be explored in the following sections.

RELATIONSHIP BETWEEN FLOW STRUCTURES

Vortical structures and their effects on heat transfer

In order to understand the relationship between the flow structures and heat transfer, the smoke visualization was performed. The smoke from a cigarette smoke generator was gently introduced through a 1 mm diameter TYGON tube into the flow at the nozzle lip. A strobe light placed behind a glass target plate was used to illuminate the flow structures through a narrow slot. Four successive photos of Fig. 7 show the stable pairing process of the ring vortices at $f_e = 950$ Hz when $H/D = 1.125$ and $Re_D = 12\,300$, which corresponds to the case of the heat transfer reduction. The shear layer starts to roll up to form the discrete vortices before it impinges on the plate wall. Then, the vortices move in the radial direction along the wall. Because the excitation frequency f_e is close to the subharmonic of the natural frequency, two vortices merge to form a bigger and stronger vortex at $r/D = 1.7$. The coalescence of two vortices is similar to that in the free jet, except that the trajectories of the vortices are deflected by the plate. After the vortex pairing, the resulting strong vortex in the outer shear layer induces a counter-rotating secondary vortex from the boundary layer at $r/D = 1.8$–2.0. The appearance of the secondary vortex can be identified in photos 1 and 4 of Fig. 7. The secondary vortices induced by the large-scale vortices in a round impinging jet have been observed by Popiel and Trass [10]. This phenomena is also referred to the vortex-induced unsteady separation which is initiated by the unsteady adverse pressure gradient produced by the primary vortex [8]. The location of the vortex-induced unsteady separation coincides with the valley of the heat transfer distribution ($r/D = 1.8$–2.0) at $f_e = 950$ Hz in Fig. 5. This suggests that the vortex-induced unsteady separation may induce the local heat transfer reduction. A significant decrease in heat transfer rate was also found by Rivir *et al.* [29] in a region of turbulent separation induced by an adverse pressure gradient on a flat surface.

In contrast with the case of $f_e = 950$ Hz, the 1750 Hz excitation produces 'intermittent' vortex pairing rather than the stable vortex pairing, as shown in Fig. 8(a). The video tape indicates that the vortices jitter in space during the intermittent vortex pairing although the jittering cannot be seen in a single frame of the photo in Fig. 8(a). In this case, the time trace

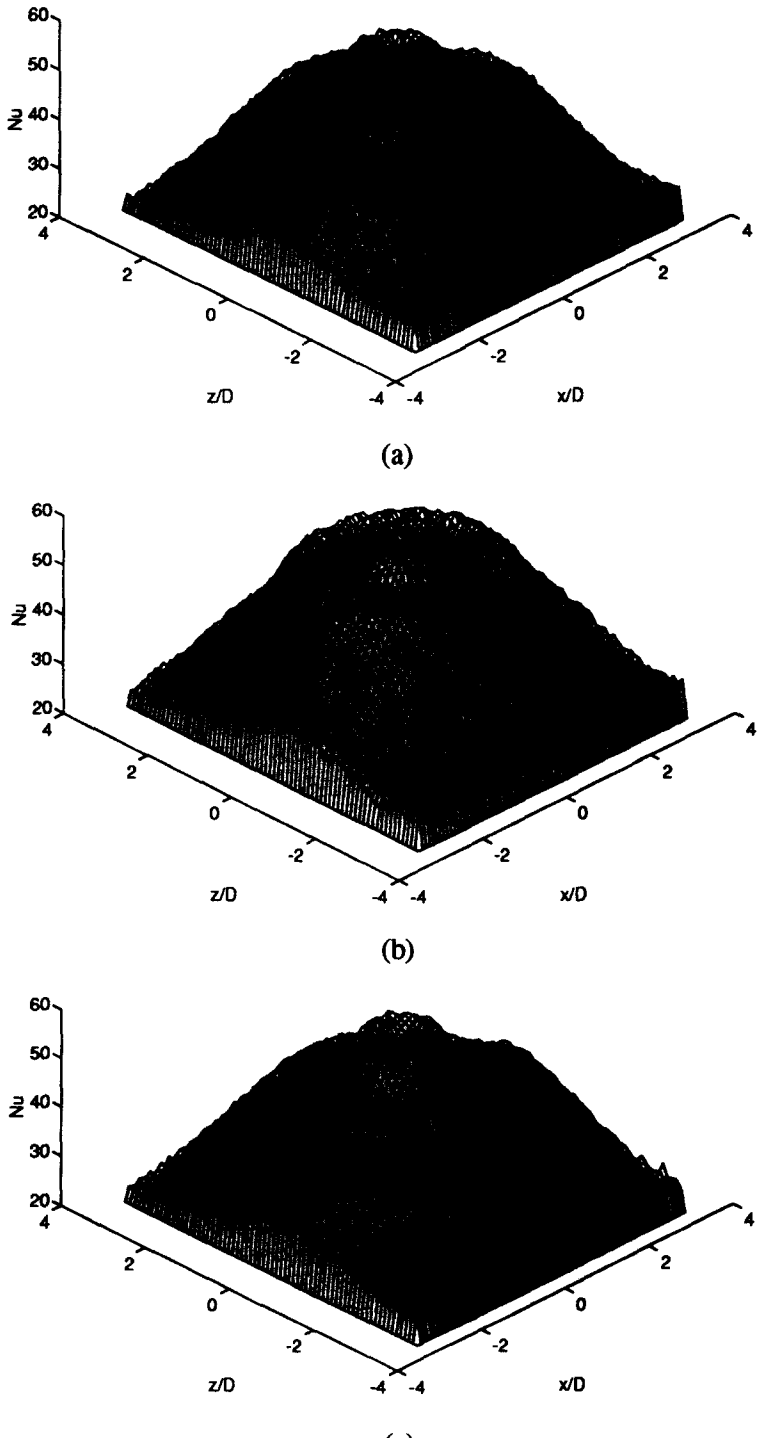

Fig. 4. Two-dimensional Nusselt number distributions of excited impinging jet when $H/D = 1.125$ and $Re_D = 12\,300$: (a) $f_e = 950$ Hz, (b) $f_e = 1750$ Hz, (c) unexcited.

of the hot-film signal shows that the subharmonic wave occurs intermittently. Also, the phase difference between the excited fundamental and self-generated subharmonic waves randomly drifts. Instead of a well-organized vortex, the intermittent vortex pairing forms a chaotic 'lump eddy' which contains a great deal of small-scale random turbulence (the term 'eddy' is used instead of 'vortex' since the flow structure is not well-organized). The vortical structures become less organized after the intermittent vortex pairing. In this case, the flow visualization does not show obvious vortex-induced separation. The location of the chaotic

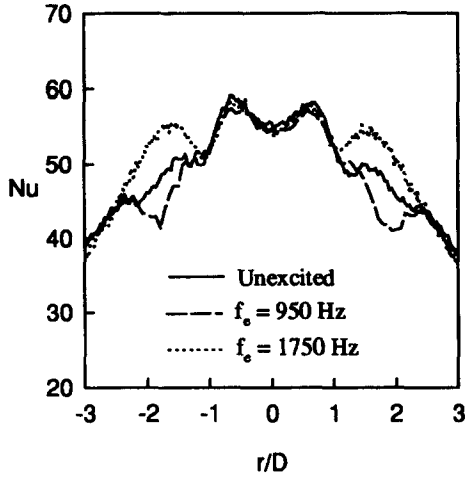

Fig. 5. Transverse Nusselt number distributions of excited impinging jet when $H/D = 1.125$ and $Re_D = 12\,300$.

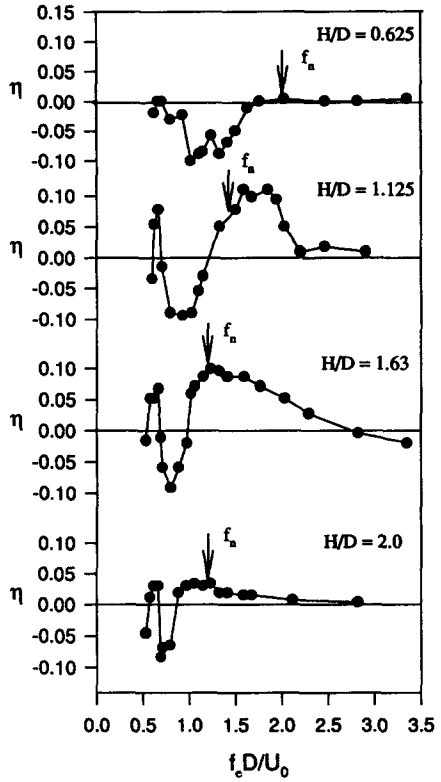

Fig. 6. Heat transfer enhancement factor as a function of excitation frequency at $r/D = 1.53$ when $Re_D = 12\,300$.

'lump eddy' just corresponds to the second peak of the heat transfer distribution ($r/D = 1.5$–1.8) at $f_e = 1750$ Hz in Fig. 5. This suggests that an increase in the random turbulence causes the heat transfer enhancement. A similar observation has been reported by Kataoka *et al.* [12]. They found that the turbulent, less coherent structure can enhance the stagnation-point heat transfer more effectively than the non-turbulent coherent structure with the periodic fluctuation. For the unexcited impinging jet at

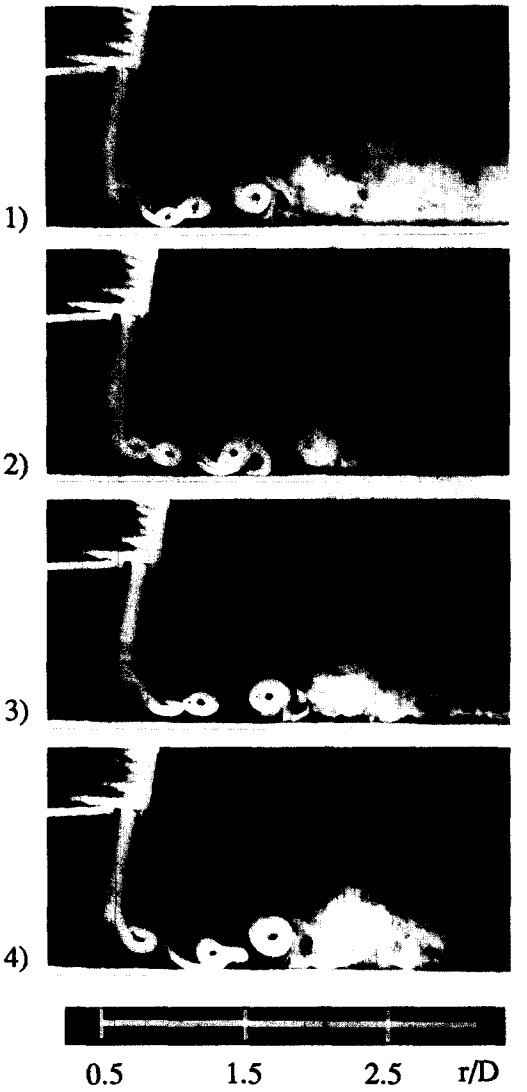

Fig. 7. Successive photos of stable vortex pairing in excited impinging jet at $f_e = 950$ Hz when $H/D = 1.125$ and $Re_D = 12\,300$.

$H/D = 1.125$, the organized vortices are shown in Fig. 8(b). No vortex pairing is observed in this case.

It is desirable to discuss effects of the large-scale organized vortices and small-scale random turbulence on heat transfer in the wall–jet region. The heat flux Q is expressed as a sum of three terms $Q = -k\partial\bar{T}/\partial y + \rho c_p\overline{v_c'T_c'} + \rho c_p\overline{v_{ic}'T_{ic}'}$, where the subscripts c and ic represent the coherent component induced by the organized vortices and incoherent component caused by the small-scale random turbulence, respectively. The first term in the right-hand side is the mean heat flux, the second term represents the coherent part of the turbulent heat flux, and the third term denotes the incoherent part of the turbulent heat flux. It should be emphasized that the first term $-k\partial\bar{T}/\partial y$ is implicitly dependent on the coherent and random fluctuating velocities, because these fluctuations modify the mean flow. For a hot wall, large-

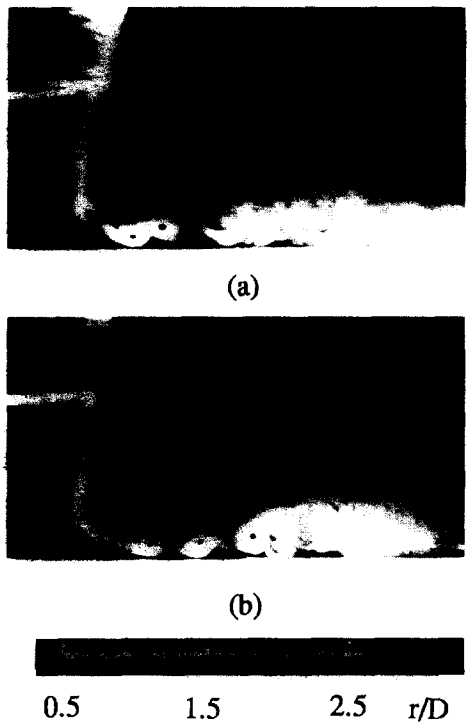

Fig. 8. Vortical structures of impinging jet when $H/D = 1.125$ and $Re_D = 12300$: (a) $f_e = 1750$ Hz, (b) unexcited.

scale mixing caused by the organized vortices has dual effect on the local heat transfer. The organized vortices in the wall–jet region entrain the colder ambient fluid into the wall boundary layer and eject the hot fluid away from the wall such that the wall is cooled. Hence, the large-scale mixing tends to enhance the local heat transfer and the local coherent heat flux $\rho c_p \overline{v_c' T_c'}$ is positive. On the other hand, the organized vortices engulf ambient fluid with low momentum and move it to the wall so as to decrease the mean shear rate in the wall boundary layer, and even induce local separation if the vortices are strong enough. Thus, the large-scale mixing reduces to the mean heat flux $-k\partial\bar{T}/\partial y$ by modifying the mean flow. The heat transfer in the wall–jet region depends on the competition between these two opposite effects associated with the large-scale organized vortices. In contrast, the small-scale random turbulence near the wall augments the mean shear rate and also generates positive incoherent heat flux $\rho c_p \overline{v_{ic}' T_{ic}'}$ at the wall. Hence, the small-scale turbulence always tends to enhance the local heat transfer. In the case of $f_e = 950$ Hz, the reduction of the mean heat flux $-k\partial\bar{T}/\partial y$ due to the vortex-induced separation overwhelms any heat transfer increase produced by the coherent heat flux $\rho c_p \overline{v_c' T_c'}$ and incoherent heat flux $\rho c_p \overline{v_{ic}' T_{ic}'}$. Thus, the local heat transfer is reduced. In the case of $f_e = 1750$ Hz, a great deal of the small-scale random turbulence is generated after the organized vortices are broken down during the intermittent pairing. The resultant small-scale random turbulence not only prevents the wall boundary layer from separation, but also significantly increases the incoherent heat flux $\rho c_p \overline{v_{ic}' T_{ic}'}$. Overall, the local heat transfer is enhanced in this case.

Heat transfer spectra

The dynamic aspects of the impinging jet can be further studied by examining spectra of the time-dependent heat transfer fluctuation. The local heat transfer fluctuation was measured by a flush-mount hot-film sensor. The spectrum development of the relative heat transfer fluctuation Q'/Q_0 at different radial locations on the wall is shown in Fig. 9(a) for the case of $f_e = 950$ Hz and $H/D = 1.125$ (heat transfer reduction case), where Q_0 is the mean heat transfer rate at the stagnation-point. For comparison, the corresponding heat transfer spectra of the unexcited impinging jet are also plotted. In all spectra for the excited impinging jet the excitation frequency f_e component is dominant, although the harmonics and weak randomness are present. Since f_e is close to the subharmonic of the natural frequency, the excitation promotes vortex pairing as indicated by the flow visualization. Compared with the unexcited case, the 950 Hz excitation considerably suppresses the broad spectral components of the small-scale random turbulence such that the well-defined characteristic frequencies f_e is still distinguishable at $r/D = 1.85$. This is consistent with the flow visualization observation which indicates the existence of the well-organized vortices at $r/D = 1.8$ after stable pairing. Figure 10(a) shows the spatial evolution of two dominant modes f_e and $2f_e$ along the radial direction. The amplitudes of the f_e and $2f_e$ modes grow exponentially at the beginning, reach a maximum at $r/D = 1$ and then decay. The total fluctuation intensity that includes the contributions from all spectral components is also given for comparison. The amplitude difference between the total intensity and discrete modes represents the amount of randomness. Figure 10(a) indicates that the f_e mode is so dominant that the flow is highly coherent for $r/D = 0.5$–1.0. Only after $r/D = 1.5$, do the broad spectral components of the small-scale random turbulence become evident. The heat transfer reduction occurs after the dominant modes saturate. Note that the f_e spectral component has a local minimum at $r/D = 1.75$ where the greatest heat transfer reduction is attained. From the flow visualization photos in Fig. 7, it can be found that the location of the amplitude minimum at $r/D = 1.75$ corresponds to the separation point between the primary vortex and the induced secondary vortex. The secondary maximum of the f_e spectral component at $r/D = 2$ is caused by the generation of the secondary vortex. The spectral analysis supports the observation that the vortex-induced separation causes the local heat transfer reduction.

When $f_e = 1750$ Hz (heat transfer enhancement case), the subharmonic component $f_e/2$ is spontaneously generated and has a comparable amplitude to the excited fundamental mode f_e over a range of

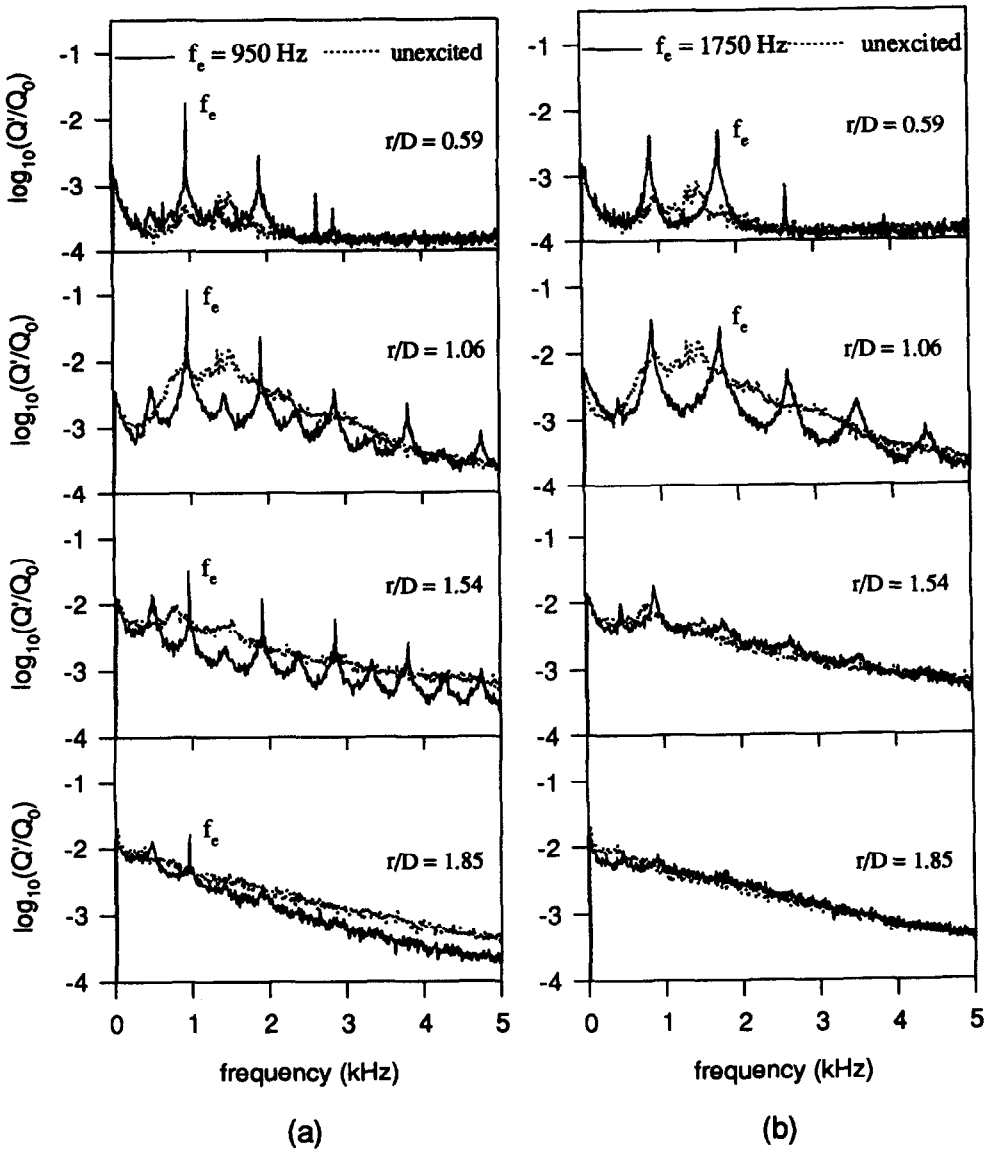

Fig. 9. Spectra of heat transfer fluctuation in excited impinging jet when $H/D = 1.125$ and $Re_D = 12\,300$: (a) $f_e = 950$ Hz, (b) $f_e = 1750$ Hz.

$r/D = 0.59$–1.06, as shown in Fig. 9(b). The self-generated subharmonic wave tends to promote the vortex pairing. However, since the amplitude and phase of the self-generated subharmonic wave usually vary, the initiated vortex pairing is not a stable process in this case. The intermittent vortex pairing has been shown in the flow visualization. At $r/D = 1.54$, the excited fundamental mode f_e is almost buried beneath the broad spectral components and only the $f_e/2$ mode is visible. This spectrum corresponds to the formation of the chaotic 'lump eddy' after the intermittent vortex pairing. When $r/D > 1.54$, all discrete spectral peaks disappear and the spectra becomes continuous, which signify fully turbulent flow. Compared with the distinct spectral peaks in the case of $f_e = 950$ Hz (heat transfer reduction case), the spectra for $f_e = 1750$ Hz reflect the rapidly vanishing organized structures when $r/D > 1.54$. As shown in Fig. 10(b), the f_e and $f_e/2$ modes experience the exponential growth until $r/D = 1$. The greater difference between the total turbulence intensity and amplitudes of the discrete modes indicates that there are more random components when $f_e = 1750$ Hz than $f_e = 950$ Hz. The heat transfer enhancement at $f_e = 1750$ Hz is achieved after the dominant modes decay after $r/D > 1$. In summary, an increase of the random flow structures enhances the local heat transfer in the wall-jet region.

Correlation between velocity and heat transfer fluctuations

In order to provide a measure of the relationship between the velocity and heat transfer rate fluc-

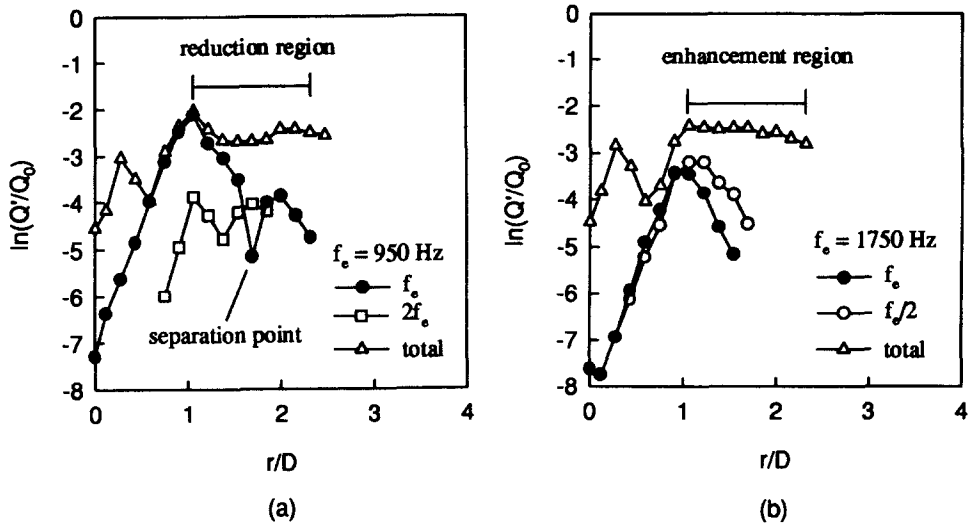

Fig. 10. Spatial evolution of dominant modes when $H/D = 1.125$ and $Re_D = 12\,300$: (a) $f_e = 950$ Hz, (b) $f_e = 1750$ Hz.

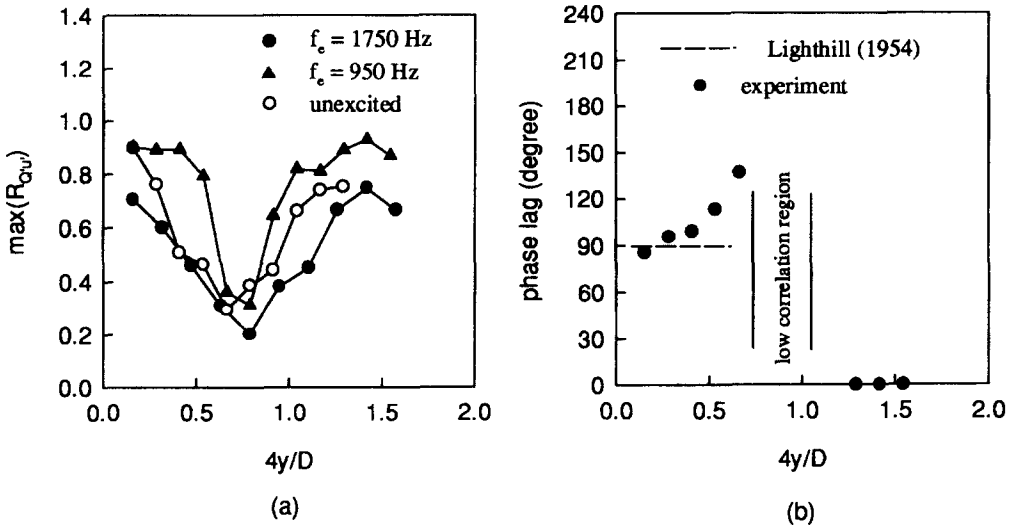

Fig. 11. Cross-correlation between velocity and heat transfer at $r/D = 1.1$ when $H/D = 1.125$ and $Re_D = 12\,300$: (a) maximum correlation coefficients, (b) phase lag of heat transfer behind velocity at $f_e = 950$ Hz.

tuations, the two-point cross-correlation coefficient $R_{Q'u'}(\tau, y)$ is used, where

$$R_{Q'u'}(\tau, y) = \overline{Q'(t+\tau, 0)u'(t, y)}/(Q'u').$$

The heat transfer rate fluctuation Q' was measured using a flush-mount hot-film sensor and the local streamwise fluctuating velocity u' was detected by a single hot-wire probe at differential vertical locations above the hot-film sensor. Figure 11(a) shows the typical distributions of the maximum correlation coefficient max $(R_{Q'u'})$ across the wall-jet at $r/D = 1.1$ and $H/D = 1.125$ in the cases of $f_e = 950$ Hz, 1750 Hz and no excitation. The distributions of max $(R_{Q'u'})$ in three cases share similar characteristics. The correlation coefficients are large near the wall and in the outer region $(4y/D > 1)$, whereas the low correlation coefficients are obtained in the intermediate region from $4y/D = 0.6$–0.9. Actually, the low correlation region corresponds to the cores of the convecting well-organized vortices. When the hot-wire probe is placed in the region where the vortex cores pass through, the time series records of the streamwise fluctuating velocity u' exhibit the complicated details of the local flow, unlike the more regular flush-mount hot-film

signal Q' representing the integral effects of the well-organized vortices. Hence, $R_{Q'u'}$ decreases there. In the outer region ($4y/D > 1$), since u' is induced by the well-organized vortices through the Biot–Savart law, the behavior of u' is similar to Q' and therefore, the value of $R_{Q'u'}$ is large. In general, the wall heat transfer rate tends to lag behind the velocity due to thermal inertia. Figure 11(b) shows the phase difference between the wall heat transfer and velocity at $r/D = 1.1$ when $f_e = 950$ Hz. The phase lag is about 90° near the wall and tends to increase with y. The phase angle jumps 150° across the low correlation region that corresponds to the cores of the vortices. The analysis of Lighthill [30] indicates that there is a phase lag of 90° for the boundary layer with the small amplitude harmonic oscillating external flow. The correlation measurements were also made at $r/D = 0.79$ and 1.5. These measurements indicate that the large-scale organized vortices dominate the heat transfer fluctuations on the surface when $r/D \leqslant 1.5$. In all cases, the correlation coefficients in the case of $f_e = 950$ Hz are obviously higher than those in the cases of $f_e = 1750$ Hz and no excitation. The u' and Q' signals when $f_e = 950$ Hz are much more coherent than other cases. It is specially noted that the excitation at $f_e = 1750$ Hz leads to even lower correlation than the unexcited impinging jet. These results are consistent with the flow visualization and spectrum analysis.

CONCLUSIONS

At small nozzle-to-plate spacing ($H/D \leqslant 2$), the local heat transfer in the wall–jet region can be significantly affected by forcing the impinging jet, whereas the heat transfer near the stagnation-point remains unchanged. The phenomena of heat transfer enhancement and reduction are related to the developments of the large-scale vortical structures in the wall–jet region. When the excitation frequency is close to the natural frequency of the impinging jet, the initiated intermittent vortex pairing produces the chaotic 'lump eddy' which contains a great deal of the small-scale random turbulence. The random vortical structures enhance the local heat transfer. When the forcing is near the subharmonic of the natural frequency, stable vortex pairing is promoted. The strong large-scale well-organized vortices formed after the stable pairing induce the unsteady separation of the wall boundary layer and hence, lead to the local heat transfer reduction.

Acknowledgements—The authors would like to thank R. Viskanta and S. P. Schneider for their comments.

REFERENCES

1. R. Viskanta, Heat transfer to impinging isothermal gas and flame jets, *Expl Thermal Fluid Sci.* **6,** 111–134 (1993).
2. K. Jambunathan, E. Lai, M. A. Moss and B. L. Button, A review of heat transfer data for single circular jet impingement, *Int. J. Heat Fluid* **13,** 106–115 (1992).
3. S. Goldstein, *Modern Developments in Fluid Dynamics*, Vols 1 and 2. Oxford University Press, Oxford (1938).
4. M. C. Smith and A. M. Kuethe, Effects of turbulence on laminar skin friction and heat transfer, *Phys. Fluids* **9,** 2337–2344 (1966).
5. C. J. Hoogendoorn, The effect of turbulence on heat transfer at a stagnation point, *Int. J. Heat Mass Transfer* **20,** 1333–1338 (1977).
6. K. Kataoka, M. Suguro, H. Degawa, K. Maruo and I. Mihata, The effect of surface renewal due to large-scale eddies on jet impingement heat transfer, *Int. J. Heat Mass Transfer* **30,** 559–567 (1987).
7. C. M. Ho and N. S. Nosseir, Dynamics of an impinging jet. Part 1, the feedback phenomenon, *J. Fluid Mech.* **105,** 119–142 (1981).
8. N. Didden and C. M. Ho, Unsteady separation in a boundary layer produced by an impinging jet, *J. Fluid Mech.* **160,** 235–256 (1985).
9. C. C. Landreth and R. J. Adrian, Impingement of a low Reynolds number turbulent circular jet onto a flat plate at normal incidence, *Exp. Fluids* **9,** 74–84 (1990).
10. C. O. Popiel and O. Trass, Visualization of a free and impinging round jet, *Expl Thermal Fluid Sci.* **4,** 253–264 (1991).
11. I. B. Özdemir and J. H. Whitelaw, Impingement of an axisymmetric jet on unheated and heated flat plates, *J. Fluid Mech.* **240,** 503–532 (1992).
12. K. Kataoka, H. Ase and N. Sako, Unsteady aspects of large-scale coherent structures and impingement heat transfer in round air jets with and without controlled excitation, *Int. J. Engng Fluid Mech.* **1,** 365–382 (1988).
13. P. J. Disimile, Effect of impinging jet excitation on curved surface heat transfer, *J. Propulsion Power* **10,** 293–294 (1993).
14. F. P. Incropera and D. P. DeWitt, *Fundamentals of Heat and Mass Transfer* (3rd Edn), Chap. 9. Wiley, New York (1990).
15. T. Liu, B. T. Campbell and J. P. Sullivan, Fluorescent paint for measurement of heat transfer in shock-turbulent boundary layer interaction, *Expl Thermal Fluid Sci.* **10,** 101–112 (1995).
16. T. Liu, B. T. Campbell and J. P. Sullivan, Surface temperature of a hot film on a wall in shear flow, *Int. J. Heat Mass Transfer* **37,** 2809–2814 (1994).
17. T. Liu, B. T. Campbell, J. P. Sullivan, J. Lafferty and W. Yanta, Heat transfer measurement on a waverider at Mach 10 using fluorescent paint, *J. Thermophys. Heat Transfer* **9,** 605–611 (1995).
18. T. Liu, B. T. Campbell and J. P. Sullivan, Accuracy of temperature-sensitive fluorescent paint for heat transfer measurements, AIAA Paper 95-2042 (1995).
19. M. J. Lighthill, Contributions to the theory of heat transfer through a laminar boundary layer, *Proc. R. Soc. Lond A* **202,** 359–377 (1950).
20. H. Liepmann and G. Skinner, Shearing stress measurements by use of a heated element, NACA TN, no. 3268 (1954).
21. C. M. Ho and P. Huerre, Perturbed free shear layers, *A. Rev. Fluid Mech.* **16,** 365–424 (1984).
22. P. A. Monkewitz and P. Huerre, Influence of the velocity ratio on the spatial instability of mixing layers, *Phys. Fluids* **25,** 1137–1143 (1982).
23. V. Kibens, Discrete noise spectrum generated by an acoustically excited jet, *AIAA J.* **18,** 434–441 (1980).
24. S. C. Crow and F. H. Champagne, Orderly structure in jet turbulence, *J. Fluid Mech.* **48,** 547–591 (1971).
25. F. K. Browand and J. Laufer, The role of large-scale structures in the initial development of circular jets, *Proceedings of the Fourth Biennial Symposium on Turbulence* (Edited by J. L. Zakin and G. K. Patterson), pp. 333–345. University of Missouri-Rolla, (1975).

26. F. O. Thomas, Structure of mixing layers and jets, *Appl. Mech. Rev.* **44,** 119–153 (1991).
27. L. C. Burmeister, *Convective Heat Transfer* (2nd Edn), Chap. 5. Wiley New York (1993).
28. P. S. Shadlesky, Stagnation point heat transfer for jet impingement to a plane surface, *AIAA J.* **21,** 1214–1215 (1983).
29. R. B. Rivir, J. P. Johnston and J. K. Eaton, Heat transfer on a flat surface under a region of turbulent separation, *J. Turbomach.* **116,** 57–62 (1994).
30. M. J. Lighthill, The response of laminar skin friction and heat transfer to fluctuations in the stream velocity, *Proc. R. Soc. Lond. A* **224,** 1–23 (1954).